Thin Solid Films 685 (2019) 1–7

Contents lists available at ScienceDirect

Thin Solid Films

journal homepage: www.elsevier.com/locate/tsf

Dopant-defect interactions in highly doped epitaxial Si:P thin films

Z.N. Weinrich[a,*], X. Li[b], S. Sharma[b], V. Craciun[c], M. Ahmed[a], E.A.C. Sanchez[b], S. Moffatt[b], K.S. Jones[a]

[a] *Department of Materials Science and Engineering, 100 Rhines Hall, University of Florida, Gainesville, Florida 32611, USA*
[b] *Applied Materials, 974 E Arques Ave. Sunnyvale California, 94085, USA*
[c] *National Institute for Laser, Plasma and Radiation Physics, Atomistilor Street, No. 409, Magurele City, Ilfov County RO-077125, P.O. Box MG-36, Romania*

ABSTRACT

Clustering configurations and reactions within in-situ doped epitaixal Si:P films were investigated. In-situ highly doped epitaxial Si:P films (HDSiP) were grown by reduced-pressure chemical vapor deposition with phosphorus concentrations up to 4.4×10^{21} cm^{-3}. Additional P activation in Si:P films into metastable states can be achieved by a 1200 °C millisecond laser anneal with negligible dopant diffusion. Dopant deactivation takes place readily during subsequent low temperature annealing for HDSiP despite negligible diffusion during the same time. Diffusion analysis of buried marker layers suggest a high concentration of interstitials being released from HDSiP and Si:P layers doped with sub 1×10^{21} cm^{-3} P concentrations. Upon thermal annealing. In addition, extrinsic dislocation loop formation was observed in sufficiently high P concentration HDSiP films. It is proposed that a high concentration of grown-in P-interstitial clusters exist concurrently with vacancy clusters theorized in HDSiP thin films.

1. Introduction

In the search for higher performance materials to fabricate next generation silicon microelectronic devices, epitaxially grown highly doped Si:P (HDSiP) has been a recent material of interest [1–9]. With a P concentration exceeding 1×10^{21} cm^{-3}, HDSiP has the potential to facilitate next generation transistor nodes due to the ability to create ultra-low contact resistance at the source/drain regions [1,2]. Another beneficial property of HDSiP is the ability to place the channel region of n-type metal-oxide-semiconductor (nMOS) transistors into a state of tensile strain for improved channel electron mobility [3,4,8]. Originally Si:C and Si:CP strained epitaxially grown layers were investigated before attention was diverted to Si:P films which can achieve comparable levels of strain as in C doped films [6,10]. For facile comparison to C doped films, biaxial tensile strain in source/drain epitaxy materials is reported in terms of equivalent at.% C_{sub}. Equivalent at.% C_{sub} is the percentage of C in Si required to achieve a given magnitude of tensile strain. Incomplete P activation and lack of visible defects observed in high resolution transmission electron microscopy (HR-TEM) micrographs of as-grown HDSiP film suggest that sub-microscopic clusters of inactive phosphorus exist in HDSiP [8]. Previous reports of similarly high P concentrations obtained via solid source diffusion or ion implantation have manifested in orthorhombic or monoclinic precipitates of SiP which have not been observed in this material [11–13]. Phase diagram data of the Si—P system doesn't show experimental evidence of a macroscale stable cubic phase mixture of Si and P above 1.2×10^{21} cm^{-3} P existing under equilibrium conditions [14]. However, the growth process used to grow these epitaxially grown films operates far from equilibrium regimes [4]. Osugi et al. reported the growth of a cubic zinc-blende SiP structure under a high temperature high pressure growth, however with minimal analysis beyond a lattice constant from X-ray diffraction (XRD). No further investigations have been reported for this compound [15]. Experimental observations of potential secondary dispersed phases are inadequate to explain the lack of precipitation in HDSiP. Density functional theory (DFT) simulations have been employed to predict stable clustering configurations of P & Si at P concentrations above 1×10^{21} cm^{-3} [5,9,16–20]. These simulations suggest that the most stable cubic configuration of Si and P in HDSiP is a pseudocubic Si_3P_4 phase (also referred to as P_4V clusters) which would have a negative enthalpy of formation [16–19]. Vegard's law calculations taking into account the predicted bulk lattice constant of Si_3P_4 from DFT agree with the observed strain for various concentrations of HDSiP films [3]. For these reasons, a dispersed Si_3P_4 phase is theorized to be present, grown into HDSiP as the sub-microscopic cluster type responsible for inactive P [3,4].

Further DFT work has suggested that P_4V clusters may not be required to obtain the observed layer strain and that dispersed substitutional P atoms could also achieve similar strain [9]. This finding is at odds with most experimental trends for lattice parameter contraction due to P doping [21–24]. It is very possible that the current literature trends underestimate strain as precipitates should be present for diffusion doped samples above 1.2×10^{21} cm^{-3} P [14,25,26]. Lattice

* Corresponding author.
E-mail address: zweinrich@ufl.edu (Z.N. Weinrich).

https://doi.org/10.1016/j.tsf.2019.05.059
Received 5 November 2018; Received in revised form 25 May 2019; Accepted 26 May 2019
Available online 28 May 2019
0040-6090/ © 2019 Published by Elsevier B.V.

parameter measurements on grown crystals with high P concentrations are an exception to the aforementioned trends as reported by Celotti et al. [27]. However, this trend has to be grossly extrapolated from the highest concentration sample studied to compare with strain values for HDSiP.

For its intended use as an nMOS source and drain material, the most important property of HDSiP is to reduce contact resistance at source/drain. Contact resistance is inherently dependent on the active carrier concentration within the source/drain material. For HDSiP, effective activation has been reported with negligible diffusion through exposure to a 0.25 millisecond (ms) laser anneal [4,7]. This anneal can increase the electrically active concentration of phosphorus from $\sim 2 \times 10^{20}\,cm^{-3}$ as-grown to levels as high as $9.8 \times 10^{20}\,cm^{-3}$ after a 1200 °C ms laser anneal [7]. Although the mechanism for this activation process is not well known it still presents a promising approach to creating very low resistance contacts. There are concerns about the effects of subsequent thermal treatments on the stability of these hyper activated layers and there have been no studies to date on this topic. The goal of this work is to gain further experimental understand about the clustering configurations within HDSiP and to investigate the mechanisms behind activation and deactivation of HDSiP thin films.

2. Experimental details

40–85 nm thick epitaxially grown films with the P concentrations used in this work were grown on nominally p-type 300 mm (001) Si wafers using an Applied Materials® Centura® reduced pressure chemical vapor deposition system. The substrate temperature for growth was maintained below 700 °C. The growth pressure was maintained between 10^3 Pa and 10^5 Pa. The growth rates used were between 10 and 100 Å/min. For samples with buried P marker layers, 5 nm thick, $\sim 5 \times 10^{19}\,cm^{-3}$ P epitaxial marker layers were grown on nominally p-type 300 mm (100) wafers. Following this, ~150 nm nominally undoped epitaxial Si was grown on top of the marker layer to serve as a spatial buffer for diffusion measurements. Finally, epitaxial SiP surface layers 50–80 nm thick were grown with concentrations of $5.0 \times 10^{20}\,cm^{-3}$ P (Low doped Si:P, or LDSiP), $1 \times 10^{21}\,cm^{-3}$ P, $2 \times 10^{21}\,cm^{-3}$ P and $4.4 \times 10^{21}\,cm^{-3}$ P HDSiP (Fig. 1). One additional wafer was created to serve as a control where no HDSiP surface layer was deposited (Fig. 1.). This sample consists only of a marker layer and spatial buffer. Growth was conducted using dichlorosilane and phosphine gas as precursors for Si and P respectively. Half of each wafer was then annealed using an Applied Materials Vantage® Astra™ dynamic surface laser annealing system at 1200 °C to further activate dopants. Samples were then cleaved into 1 cm × 1 cm coupons and the native oxide removed by dipping in dilute HF. A standard three-step solvent process was employed to ensure a clean surface for the pressed-on indium wire electrical contacts used to conduct Hall-effect measurements.

2.1 Analytical Methods.

Hall-effect measurements were taken using an MMR Technologies variable temperature Hall system using an H-50 controller and an MPS-50 power supply. Measurements were taken at room temperature. A Hall factor of 1 has been assumed for this work. Annealing was either done using an AG Associates Heatpulse 4100 rapid thermal annealing (RTA) system or a tube furnace under inert ambient. Thermal oxidation was conducted using an atmosphere of dry O_2 in a tube furnace or using an AG Associates Heatpulse 4100 for rapid thermal oxidation (RTO). Secondary ion mass spectrometry (SIMS) was conducted by Evans Analytical using a Cs^+ primary beam. The Florida object-oriented process simulator (FLOOPS) was used to extract diffusivity values for P tail diffusion from SIMS profiles. Cross-sectional HR-TEM samples were prepared using a FEI Helios dual-beam focused ion beam (FIB) lithography tool and imaged on either a FEI Tecnai F20 microscope or a JEOL 2010F microscope using on-axis imaging conditions. High resolution X-ray diffraction (HR-XRD) analysis was conducted monitoring the (004) characteristic Bragg reflection using a Bruker JVX7300LSI triple-axis configuration diffractometer with a Cu K_α X-ray source.

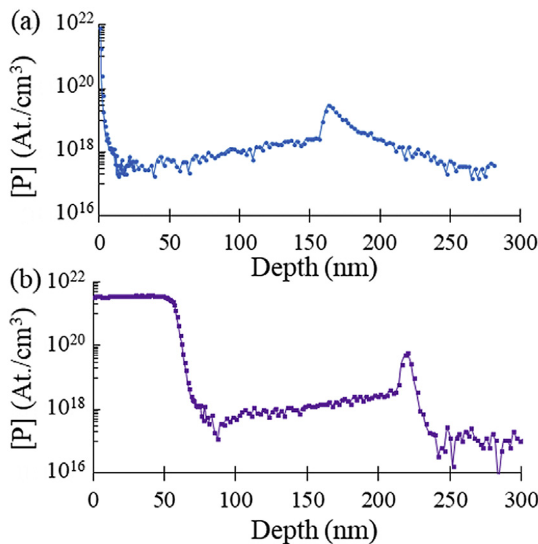

Fig. 1. (a) As-grown control marker layer sample depth profile. (b) as-grown HDSiP marker layer sample depth profile. $4.4 \times 10^{21}\,cm^{-3}$ P HDSiP sample shown.

3. Results and discussion

3.1. Dopant thermal deactivation

Dopant thermal stability experiments were undertaken by exposing samples of HDSiP to the ms laser anneal (1200 °C, 0.25 ms) to further activate dopants to metastable states. This was followed by a secondary RTA between 600 °C and 900 °C to study thermal stability. The temperatures and times chosen for this study were roughly representative of thermal budgets in a transistor process flow. HDSiP epitaxially grown layers exhibited negligible diffusion during ms laser anneal and RTA anneals up to 30 m at 700 °C as seen in Fig. 2, and thus changes in active dopant concentration in this study cannot be attributed to an increasing junction depth. Calculations using P diffusivity values from literature

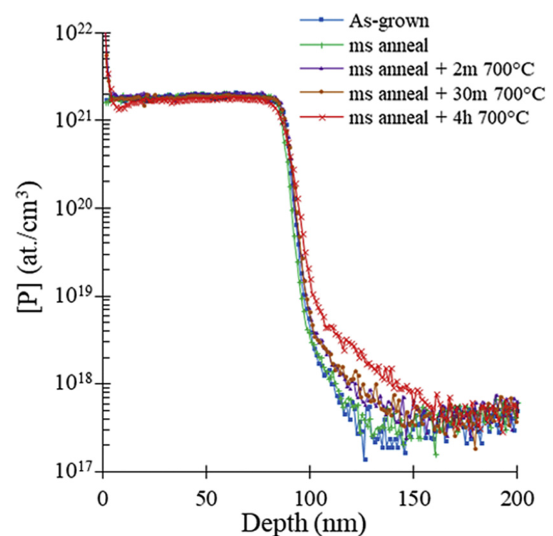

Fig. 2. SIMS dopant concentration profiles showing negligible diffusion of HDSiP layer after ms laser anneal and insignificant diffusion occurring compared to active carrier concentration within the annealing time scales studied for electrical property stability (up to 2 m). Tail diffusion can be easily discerned after 4 h at 700 °C.

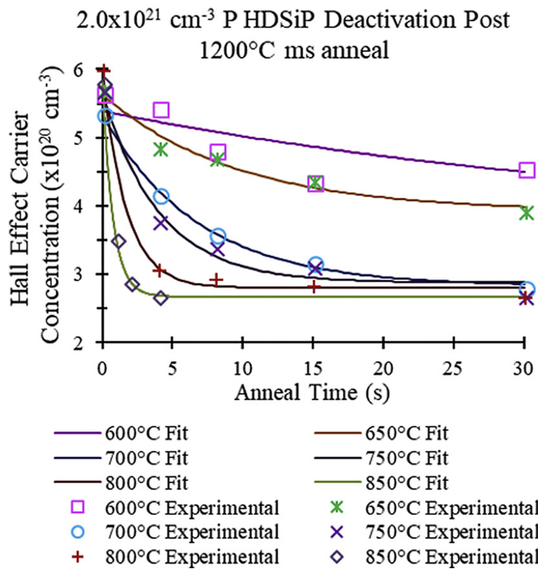

Fig. 3. Hall-effect data shows deactivation of post 1200 °C ms anneal as a function of time for HDSiP at various RTA temperatures.

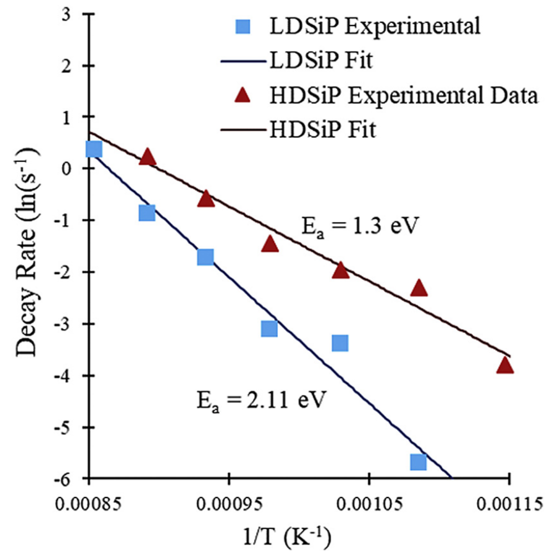

Fig. 5. Arrhenius plot showing a difference in activation energy for the deactivation process of HDSiP and LDSiP.

suggest that the higher temperature and time annealing conditions used in this study would exhibit similarly insignificant diffusion [28–30].

Active carrier concentration values were calculated from the Hall measurements using the film thickness obtained from the SIMS profile. Both LDSiP and HDSiP layers readily deactivate after a period of seconds to minutes at temperatures above 600 °C. Fig. 3 shows the observed deactivation characteristics of HDSiP as a function of temperature and time. A similar series of curves was created for the LDSiP sample (not shown). Fig. 4 compares the stability of HDSiP layers to LDSiP layers activated by ms anneal and subsequently annealed at 700 °C. For HDSiP, dopants deactivated back to as-grown levels after 60 s at 700 °C. LDSiP maintains electrical property stability for a significantly longer anneal duration. The deactivation kinetics for both HDSiP and LDSiP followed an exponential decay relationship and were fit accordingly to eq. 1 [31].

$n = y_0 + A exp(-kt)\#[1]$

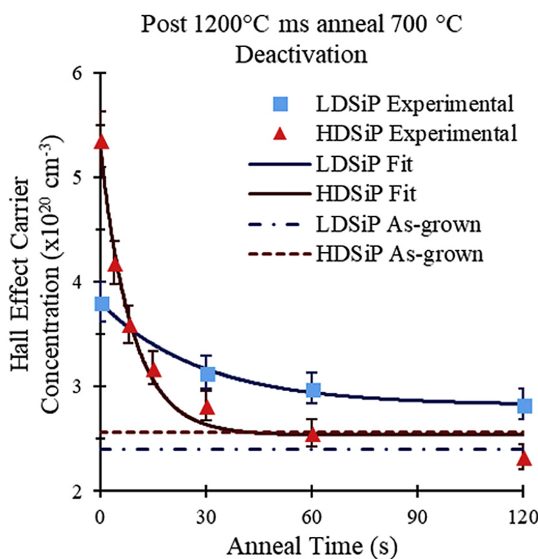

Fig. 4. Hall-effect data shows deactivation of post 1200 °C ms annealed samples as a function of time for HDSiP and LDSiP after a 700 °C RTA. As-grown active carrier concentration shown on plot for comparison and did not undergo any thermal treatment.

From this relation, a rate constant, k, was obtained for each post ms anneal RTA temperature. These rate constants were then plotted following the Arrhenius relation for temperature dependence as seen in Fig. 5. An activation energy for the deactivation process was calculated from the slope of the Arrhenius plot to be 2.1 eV for LDSiP. The activation energy for HDSiP deactivation was 1.3 eV indicating a possible shift in the mechanism for deactivation as a function of chemical dopant concentration.

Microstructural analysis was conducted on HDSiP films exposed to ms anneal and deactivating secondary anneal. In Fig. 6, HR-TEM images of the HDSiP samples show a lack extended defects or precipitation throughout ms anneal and deactivating secondary anneal. Despite significant increases in active P level after ms anneal and significant deactivation following a secondary RTA at 700 °C for 2 min in Fig. 4, no change in film crystallinity was observed by TEM. Fig. 7 suggests that the film strain measured with HR-XRD exhibits no change after single exposure to the 0.25 ms laser anneal. Additionally, no strain loss can be observed during the deactivating thermal anneal after 2 min.

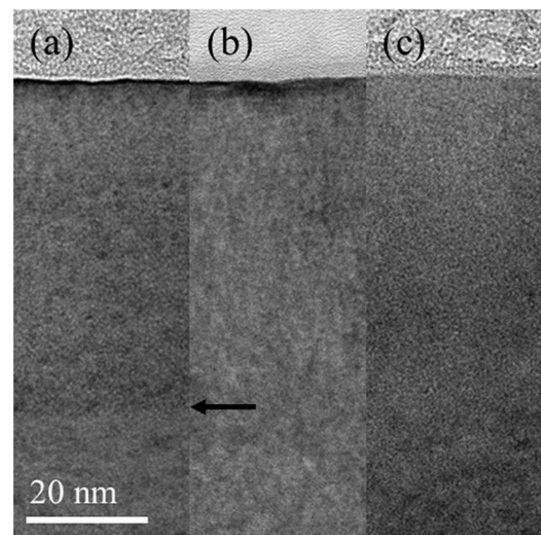

Fig. 6. HDSiP sample showing a defect free layer after the following annealing conditions: (a) As-grown (b) 1200 °C ms anneal to activate dopants (c) 1200 °C ms anneal followed by 2 m RTA at 700 °C deactivating sample to as-grown levels. The black arrow indicates the HDSiP / substrate interface depth.

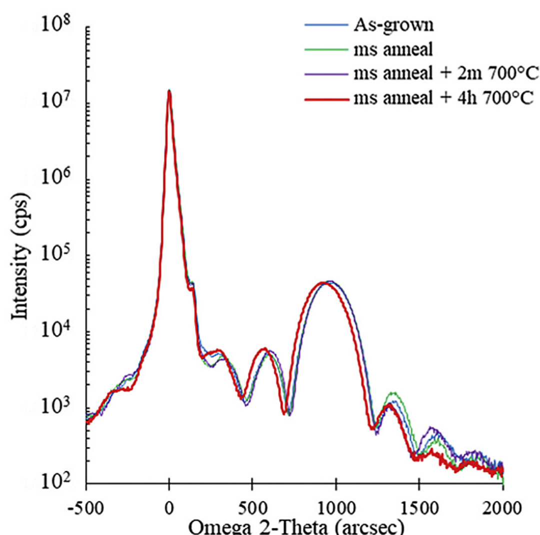

Fig. 7. HR-XRD rocking curve analysis of 2.0 × 10^{21} cm^{-3} P HDSiP films after annealing.

This suggests that if P_4V clusters are responsible for layer strain, they do not participate in activation and deactivation. After 4 h at 700 °C, where P out-diffusion from the HDSiP layer happened, slight strain loss was observed from equivalent 0.86 at.% C_{sub} to equivalent 0.84 at.% C_{sub} by HR-XRD. If P_4V clusters are not necessary to explain the layer strain, the loss of strain is explained by the diffusion of the HDSiP layer and consequent minor reduction in peak P concentration throughout the layer.

Previous reports used Rutherford backscattering spectroscopy (RBS) to suggest an increase in the concentration of P on interstitial sites however the data is excessively noisy [9]. RBS analysis was conducted in this study on 2 × 10^{21} cm^{-3} P HDSiP in the as-grown state, after ms anneal, and after ms anneal followed by a 30 min 700 °C secondary anneal. No significant variations in the aligned sample yield could be detected as a function of annealing conditions. This was the case for the layer as a whole as well as for the isolated phosphorus signal.

3.2. Dopant deactivation mechanisms

The activation energy for deactivation observed in this study for HDSiP is relatively low compared to many processes that involve the motion of a substitutional atom escaping from its lattice site [28,29,32]. Taking this into account, two possible mechanisms are considered. The first mechanism involves the breakup and reforming of vacancy clusters. This type of mechanism has been proposed in the literature to be responsible for ms laser activation of HDSiP [7,9]. For this mechanism, P_4V clusters fully or partially dissociate during laser annealing. Deactivation would proceed via the reverse reaction as no precipitation is observed in TEM. Physical mechanisms for P_4V dissociation during activation would require that outside point defects not bound to a P_4V cluster mediate the reaction. Due to the nature of the P diffusion process in Si occurring via an interstitialcy mechanism it is probable that P_4V dissolution would be an interstitial mediated process [28,29,32]. At high temperature, a free interstitial recombines with the central vacancy of a P_4V cluster causing a reduction in the vacancy population as seen by Dhayalan et al. [9]. A second interstitial would be required to disassociate a P atom from the resultant P_4 substitutional cluster causing activation of the dissociated P atom. Deactivation would follow by reforming P substitutional clusters, where the limiting step is interstitialcy diffusion to form P_4 substitutional clusters. The exact mechanism and driving force for this process is not known. Frenkel pair formation within a P_4 cluster would be spontaneous due to the energetic favorability of P_4V predicted with DFT [16,18,20].

A second deactivation mechanism proposed here does not require the activation of P from P_4V clusters and can be consistent with the theory that P_4V clusters are necessary to explain the high layer tensile strain. It is proposed that P-interstitial clusters (PICs) are grown into the HDSiP layer existing concurrently with P_4V clusters. PICs have been previously reported in the work of Keys et al. [33,34]. Appropriate ms laser anneal conditions on HDSiP does not inherently cause the film strain loss as reported in this paper. Dissolution of PICs during the ms anneal creates substitutional P and self-interstitials that form into self-interstitial clusters or fill in the vacancy of P_4V clusters. The reverse then takes place during secondary thermal treatment as free interstitials combine with substitutional P preventing electron donation. Free interstitials causing deactivation could either be from self-interstitial clusters or spontaneous Frenkel pair formation within a P_4 cluster forming a P_4V. The equilibrium between these types of clusters that exists in the as-grown state is reestablished after sufficient time of secondary annealing. It should be mentioned that this mechanism and the previously discussed P_4V dissolution mechanism involve a high concentration of interstitials. The effects of these interstitials on strain is not well understood.

For the 5 × 10^{20} cm^{-3} P LDSiP sample, more possibilities exist for deactivation mechanisms. Activation and deactivation of LDSiP may stem interstitial mediated mechanisms similar to HDSiP. However, given that a higher activation energy of 2.1 eV was observed for deactivation of LDSiP, it is suggested that the concentration of interstitials present in the LDSiP layer during deactivation has substantially decreased. Point defect release by HDSiP and LDSiP was investigated in section 2.2 to expand on this claim.

3.3. Point defect release during annealing

Diffusion enhancement of a buried dopant marker layer can serve as an indicator of point defect flux [35]. As P tail diffusion occurs via a purely interstitialcy mechanism (f_I = 0.99), diffusion enhancement of the marker layer ($D_P/D_P{}^*$) is equal to the oversaturation of interstitials ($C_I/C_I{}^*$) at the marker layer depth [28–30,32]. This approach has been used extensively to study the nature and relative concentration of point defects released during the processing of silicon [36–41]. It is possible then to discern the type and quantity of point defects released by HDSiP upon annealing. This is done by comparing the diffusion of their respective buried marker layers to a control buried marker layer sample with no surface doped layer.

For the control phosphorus marker layer sample (Fig. 1a), a diffusivity value of 7 × 10^{-19} cm^2/s was predicted at 700 °C [29]. As was expected, after 4 h of inert annealing at this temperature, negligible diffusion of the control sample marker layer can be observed from Fig. 8. After longer time anneals, significant diffusion can be observed. An average diffusivity value of 1.3 × 10^{-18} cm^2/s was obtained through modeling the diffusion behavior of samples annealed at 700 °C between 4 h and 240 h using FLOOPS. This value agrees with the value for P diffusivity of 1.4 × 10^{-18} cm^2/s at 700 °C determined by Bracht et al. [30].

A series of furnace annealing times at 700 °C was carried out on marker layer samples with a surface 2.0 × 10^{21} cm^{-3} P HDSiP layer. Fig. 9 shows the marker layer diffusion is significantly greater than was observed in the control sample (Fig. 8). The data suggests a $C_I/C_I{}^*$ value of 16 during the first 30 min. This indicates a significant release of interstitials from HDSiP. As shown in Fig. 10, the oversaturation of interstitials released from HDSiP measured at the buried marker layer depth is transient in nature. The decay time constant for this release is 136 min at 700 °C. The degree of oversaturation completely decays after a period of 4 h.

To understand the dependence of point defect release as a function of incorporated phosphorus concentration, samples with varying P concentration surface layers were annealed at 700 °C for 4 h. A similar plot to Fig. 9 can be seen for a sample with a LDSiP (5 × 10^{20} cm^{-3} P)

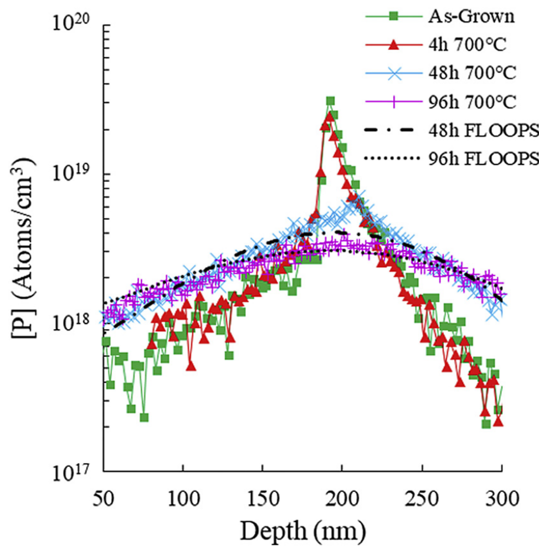

Fig. 8. Control marker layer showing negligible diffusion after 4 h at 700 °C. Substantial diffusion observed after 48 h at 700 °C. Black dashed lines are simulated diffusion profiles for P tail diffusion generated from inputting the as-grown profile into the FLOOPS diffusion simulation program showing agreement with the experimental data.

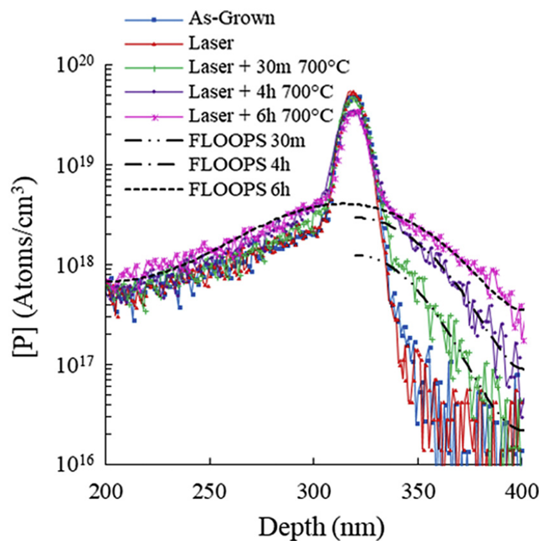

Fig. 9. Diffusion of the buried marker layer of samples with an 80 nm thick $2.0 \times 10^{21}\ cm^{-3}$ P HDSiP surface layer. Enhanced marker layer diffusion can be observed in comparison to control marker layer sample with no HDSiP surface layer (shown in Fig. 1a). Black dashed lines are simulated diffusion profiles for P tail diffusion generated from inputting the as-grown profile into the FLOOPS diffusion simulation program showing agreement with the experimental data.

surface layer in Fig. 11. A trend of decreasing interstitial release was observed with increasing P concentration before abruptly increasing for the $4.4 \times 10^{21}\ cm^{-3}$ P HDSiP sample (Fig. 12). It is not likely that a lower concentration of PICs are being grown into films with more P. Activation of HDSiP with a ms laser anneal shows a slightly increasing amount of dopant activation with increasing P concentration. As activation comes from PIC dissolution, this indicates that more PICs are grown into higher P concentration films. To explain the lower interstitial release from films with a higher concentration of grown-in interstitials, three factors are proposed.

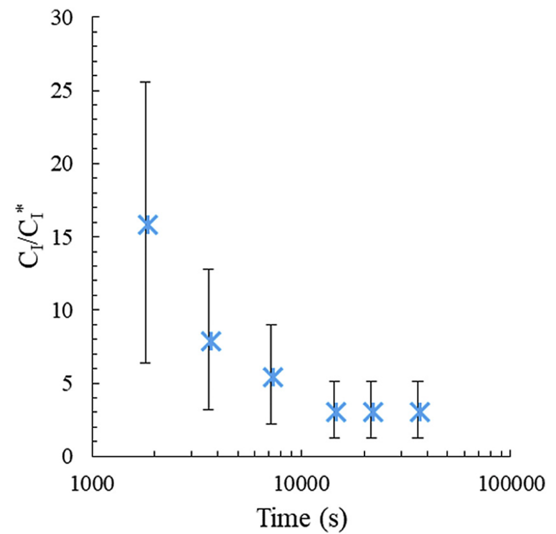

Fig. 10. Diffusivity enhancement at 700 °C shows a decay in the interstitial flux through the buried marker layer with increasing anneal time for a $2.0 \times 10^{21}\ cm^{-3}$ P HDSiP sample.

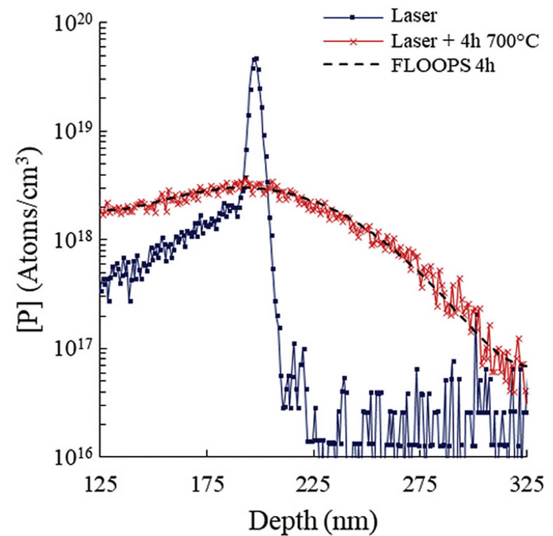

Fig. 11. Diffusion of buried P marker layer for sample with a 57 nm thick $5.0 \times 10^{20}\ cm^{-3}$ P LDSiP surface layer. Enhanced diffusion can be observed compared to control marker layer sample with no HDSiP surface layer (shown in Fig. 1a). The degree of enhancement observed is greater than that of the $2.0 \times 10^{21}\ cm^{-3}$ P HDSiP sample.

3.4. Structure property relationships in HDSiP

For a dopant that diffused via an interstitialcy mechanisms such as P, potential energy reduction favors distance minimization between interstitials and P [28]. It has been suggested in the literature that for extremely high doping levels, the possibility exists where the density of dopant atoms is too high for an interstitial within the doped region to become unassociated with any of the dopant atoms of the region [28,42]. This would create a stabilizing effect on interstitials within the doped region and an energy barrier for interstitial species to diffuse into the substrate.

Layer strain may also play a role in stabilizing interstitial clusters in HDSiP. DFT simulation work suggests that significant increases in binding energy and reductions in formation energy result for preferred size interstitial clusters when the lattice is under tensile strain [43,44]. Higher strain would further prevent interstitial diffusion out of the

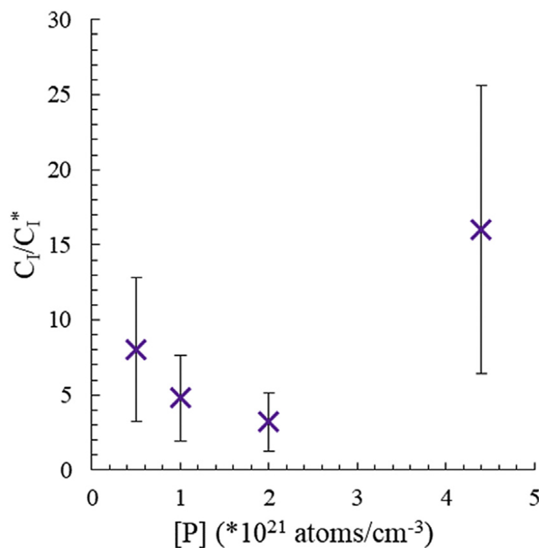

Fig. 12. Concentration dependence of interstitial release for HDSiP and LDSiP films. All samples were annealed at 700 °C for 4 h in inert ambient.

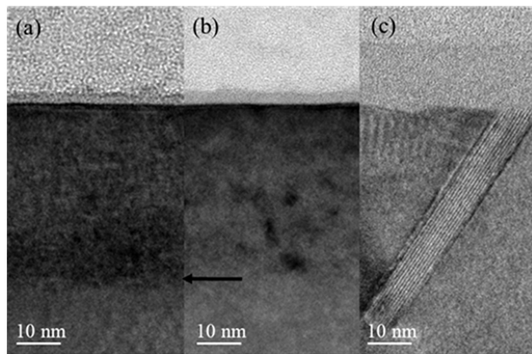

Fig. 13. HR-TEM cross sectional images of 4.4×10^{21} cm^{-3} P HDSiP sample after (a) ms laser anneal (b) ms laser anneal followed by 30 m inert anneal at 700 °C showing dislocation loop formation (c) ms laser anneal and 3 m RTO at 900 °C showing stacking fault formation. The black arrow indicates the HDSiP/substrate interface depth prior to annealing.

HDSiP strained layer as interstitials would preferentially reform into immobile clusters rather than diffuse into the substrate.

As has been discussed in Section 2.1, it is likely that ms annealing causes the central vacancy of P_4V complexes to be filled in with an interstitial. Although this configuration is energetically unstable and forms a Frenkel pair during low temperature thermal annealing of the activated film, interstitial capture by P_4V clusters is a third factor at play to explain the reduced interstitial release measured for higher P concentration HDSiP films.

In 5.0×10^{20} cm^{-3} P HDSiP, all of these aforementioned factors are significantly reduced compared to higher concentration HDSiP films and there is a greater tendency for interstitials to diffuse into the bulk. This is consistent with the deactivation data in section 2.1 where LDSiP exhibited a higher degree of active carrier stability than HDSiP films. With more interstitials leaving the LDSiP layer, fewer interstitials remain in the film to reform PICs and cause deactivation.

Above 4.4×10^{21} cm^{-3} P the diffusion enhancement abruptly increased. This film is close to the maximum incorporation of P in an HDSiP film prior to epitaxial breakdown likely caused by too high tensile strain. It is possible that as the P concentration approaches this level, a sharp increase in interstitial incorporation occurs during growth. The concentration of PICs that exist in this concentration film may be above what is possible to activate with ms laser annealing. The concentration of interstitials that are grown into 4.4×10^{21} cm^{-3} P HDSiP is above what can be stabilized leading to a higher concentration of interstitials released to the bulk than for moderately doped HDSiP.

3.5. Microstructural analysis of HDSiP

To analyze the effects of such a high concentration of interstitials, microstructure analysis was conducted on the 4.4×10^{21} cm^{-3} P HDSiP sample. The sample was observed to be defect free after ms laser annealing (Fig. 13). Upon secondary annealing at 700 °C for 30 min where the highest measured diffusivity enhancement of 40× was seen, the formation of dislocation loops was observed. No extended defects were observed to form for any P concentrations films below 4.4×10^{21} cm^{-3}. For the 4.4×10^{21} cm^{-3} sample, the average diameter of these dislocation loops was ~4 nm, too small to be characterized as intrinsic or extrinsic through use of amplitude contrast methods [45]. These are similar to the dot type defects observed by Keys et al. [33,34]. Upon oxidation at 700 °C the loops were observed to grow and eventually evolve into stacking faults during a 900 °C 3 min RTO. These results are consistent with the loops being extrinsic in nature. The formation of extrinsic defects in the 4.4×10^{21} cm^{-3} P doped sample as well as the enhanced diffusion of the marker layer both strongly suggest that at the highest doping concentrations of HDSiP the concentration of interstitials grown into the layer becomes very high.

4. Conclusions

In conclusion, dopant defect interactions in HDSiP were studied. The electrical dopant activation level observed in ms annealed HDSiP is inherently unstable upon low temperature secondary annealing. The deactivation process follows an Arrhenius behavior with a single activation energy. Deactivation kinetics were determined for LDSiP as well as HDSiP and activation energies of 2.1 eV and 1.3 eV, respectively, were obtained for the deactivation processes. Microstructure stability was analyzed using HR-TEM demonstrating that HDSiP layers remained defect free after ms anneal and post ms anneal thermal treatment. No change in the strain state of HDSiP was observed after activating or deactivating anneals before P diffusion happened at extreme conditions. It is proposed that activation and deactivation in HDSiP involves an interstitial mediated mechanism.

The point defect release by HDSiP epitaxially grown films was analyzed using a buried marker layer study. HDSiP films were observed to release a significant concentration of interstitial species supporting the claims that a high concentration of grown-in PICs is responsible for activation and deactivation in HDSiP films. Marker layer studies showed that the grown in interstitials are up to 40× above equilibrium values at 700 °C and are released from the HDSiP layer in a transient fashion. When the P concentration is increased to around 4.4×10^{21} cm^{-3}, the interstitial population is sufficient to spontaneously nucleate extrinsic dislocation loops under even low temperature anneals.

Acknowledgements

V.C. work was supported by NUCLEU-INFLPR project. We thank Dr. D. Pantelica from HH-IFIN for the RBS channeling measurements. The authors thank the Research Service Centers at the University of Florida for the use of their TEM and FIB equipment.

References

[1] C.N. Ni, X. Li, S. Sharma, K.V. Rao, M. Jin, C. Lazik, V. Banthia, B. Colombeau, N. Variam, A. Mayur, H. Chung, R. Hung, A. Brand, Ultra-low contact resistivity with highly doped Si:P contact for nMOSFET, 2015 Symp. VLSI Technol, 2015, pp. T118–T119, , https://doi.org/10.1109/VLSIT.2015.7223711 (VLSI Technol..

[2] C.N. Ni, K.V. Rao, F. Khaja, S. Sharma, S. Tang, J.J. Chen, K.E. Hollar, N. Breil, X. Li, M. Jin, C. Lazik, J. Lee, H. Maynard, N. Variam, A.J. Mayur, S. Kim, H. Chung, M. Chudzik, R. Hung, N. Yoshida, N. Kim, Ultra-low NMOS contact resistivity using a novel plasma-based DSS implant and laser anneal for post 7 nm nodes, 2016 IEEE Symp. VLSI Technol, 2016, pp. 1–2, , https://doi.org/10.1109/VLSIT.2016.7573383.

[3] Z. Ye, S. Chopra, R. Lapena, Y. Kim, S. Kuppurao, High tensile strained in-situ phosphorus doped silicon epitaxial film for nMOS applications, ECS Trans. 50 (2013) 1007–1011, https://doi.org/10.1149/05009.1007ecst.

[4] X. Li, A. Dube, Z. Ye, S. Sharma, Y. Kim, S. Chu, Selective epitaxial Si:P film for nMOSFET application: high phosphorous concentration and high tensile strain, ECS Trans. 64 (2014) 959–965, https://doi.org/10.1149/06406.0959ecst.

[5] S.K. Dhayalan, J. Kujala, J. Slotte, G. Pourtois, E. Simoen, E. Rosseel, A. Hikavyy, Y. Shimura, S. Iacovo, A. Stesmans, R. Loo, W. Vandervorst, On the manifestation of phosphorus-vacancy complexes in epitaxial Si:P films, Appl. Phys. Lett. 108 (2016), https://doi.org/10.1063/1.4942605.

[6] E. Rosseel, H.B. Profijt, A.Y. Hikavyy, J. Tolle, S. Kubicek, G. Mannaert, C. L'abbe, K. Wostyn, N. Horiguchi, T. Clarysse, B. Parmentier, S. Dhayalan, H. Bender, J.W. Maes, S. Mehta, R. Loo, T.E. Society, Characterization of epitaxial Si:C:P and Si:P layers for source/drain formation in advanced bulk FinFETs, ECS Trans. 64 (6) (2014) 977–987, https://doi.org/10.1149/06406.0977ecst.

[7] E. Rosseel, S.K. Dhayalan, A.Y. Hikavyy, R. Loo, H.B. Profijt, D. Kohen, S. Kubicek, T. Chiarella, H. Yu, N. Horiguchi, D. Mocuta, K. Barla, A. Thean, G. Bartlett, J. Margetis, N. Bhargava, J. Tolle, Selective epitaxial growth of high-P Si:P for source/drain formation in advanced Si nFETs, ECS Trans. 75 (2016) 347–359, https://doi.org/10.1149/07508.0347ecst.

[8] K.D. Weeks, S.G. Thomas, P. Dholabhai, J. Adams, Characterization and analysis of epitaxial silicon phosphorus alloys for use in n-channel transistors, Thin Solid Films 520 (2012) 3158–3162, https://doi.org/10.1016/j.tsf.2011.10.107.

[9] S. Dhayalan, J. Kujala, J. Slotte, G. Pourtois, E. Simoen, E. Rosseel, A. Hikavyy, Y. Shimura, R. Loo, W. Vandervorst, On the evolution of strain and electrical properties in as-grown and annealed Si: P Epitaxial films for source-drain stressor applications, vol. 7, (2018), pp. 228–237, https://doi.org/10.1149/2.0071805jss.

[10] H.S. Wong, K.W. Ang, L. Chan, K.M. Hoe, C.H. Tung, N. Balasubramanian, D. Weeks, M. Bauer, J. Spear, S.G. Thomas, G. Samudra, Y.C. Yeo, Silicon-carbon stressors with high substitutional carbon concentration and in situ doping formed in source/drain extensions of n-channel transistors, IEEE Electron Device Lett. 29 (2008) 460–463, https://doi.org/10.1109/LED.2008.920274.

[11] D. Nobili, A. Armigliato, M. Finnetti, S. Solmi, Precipitation as the phenomenon responsible for the electrically inactive phosphorus in silicon, J. Appl. Phys. 53 (1982) 1484–1491, https://doi.org/10.1063/1.330646.

[12] S. Solmi, A. Parisini, R. Angelucci, A. Armigliato, D. Nobili, Dopant and carrier concentration in Si in equilibrium with monoclinic SiP precipitates, Phys. Rev. B - Condens. Matter Mater. Phys. 53 (1996) 7836–7841, https://doi.org/10.1103/PhysRevB.53.7836.

[13] A. Bourret, W. Schröter, HREM of SiP precipitates at the (111) silicon surface during phosphorus predeposition, Ultramicroscopy. 14 (1984) 97–106, https://doi.org/10.1016/0304-3991(84)90113-X.

[14] G.J. Olesinski, R.W; Kanani, N.; Abbaschian, the P-Si (phosphorus-silicon) system, Bull. Alloy Phase Diagr., 6 (1985) 130–133. doi:https://doi.org/10.1007/BF02869224.

[15] Y.T. Jiro Osugi, Ryosuke Namikawa, reaction of silicon and phosphorus at high temperature and high pressure, Rev. Phys. Chem. Japan. 36 (1966) 35–43 (doi).

[16] B. Sahli, K. Vollenweider, N. Zographos, C. Zechner, K. Suzuki, Phosphorus diffusion and activation in silicon: process simulation based on ab initio calculations, Mater. Res. Soc. Symp. Proc. 1070 (2008) 105–110, https://doi.org/10.1557/PROC-1070-E03-03.

[17] B. Sahli, K. Vollenweider, W. Fichtner, Ab initio calculations for point defect clusters with P, As, and Sb in Si, Phys. Rev. B - Condens. Matter Mater. Phys. 80 (2009) 1–8, https://doi.org/10.1103/PhysRevB.80.075208.

[18] M. Huang, Y.P. Feng, A.T.L. Lim, J.C. Zheng, Structural and electronic properties of Si3P4, Phys. Rev. B 69 (2004) 054112, , https://doi.org/10.1103/PhysRevB.69.054112.

[19] M. Xu, S. Wang, G. Yin, L. Chen, Y. Jia, Theoretical investigation of the electronic and optical properties of pseudocubic Si3P4, Ge3P4 and Sn3P4, Opt. Express 14 (2006) 710–716, https://doi.org/10.1364/OPEX.14.000710.

[20] T.Y. Lü, J.C. Zheng, Electronic properties of pseudocubic IV-V compounds with 3:4 stoichiometry: chemical trends, Chem. Phys. Lett. 501 (2010) 47–53, https://doi.org/10.1016/j.cplett.2010.10.055.

[21] G.L. Pearson, J. Bardeen, Electrical properties of pure silicon and silicon alloys containing boron and phosphorus, Phys. Rev. 75 (1949) 865–883, https://doi.org/10.1103/PhysRev.75.865.

[22] B.G. Cohen, X-ray measurement of elastic strain and lattice constant of diffused silicon, Solid State Electron. 10 (1967) 33–37, https://doi.org/10.1016/0038-1101(67)90110-4.

[23] K. Yagi, N. Miyamoto, J.I. Nlshizawa, Anomalous diffusion of phosphorus into silicon, Jpn. J. Appl. Phys. 9 (1970) 246, https://doi.org/10.1143/JJAP.9.246.

[24] K.G. McQuhae, A.S. Brown, The lattice contraction coefficient of boron and phosphorus in silicon, Solid State Electron. 15 (1972) 259–264, https://doi.org/10.1016/0038-1101(72)90079-2.

[25] F.A. Trumbore, Solid Solubilities of impurity elements in germanium and silicon, Bell Syst. Tech. J. 39 (1960) 205–233, https://doi.org/10.1002/j.1538-7305.1960.tb03928.x.

[26] V.E. Boeisenko, S.G. Yudin, Steady-state solubility of substitutional impurities in silicon, Phys. Status Solidi 101 (1987) 123–127, https://doi.org/10.1002/pssa.2211010113.

[27] G. Celotti, D. Nobili, P. Ostoja, Lattice parameter study of silicon uniformly doped with boron and phosphorus, J. Mater. Sci. 9 (1974) 821–828, https://doi.org/10.1007/BF00761802.

[28] P.M. Fahey, P.B. Griffin, J.D. Plummer, Point defects and dopant diffusion in silicon, Rev. Mod. Phys. 61 (1989) 289–384, https://doi.org/10.1103/RevModPhys.61.289.

[29] P. Pichler, Intrinsic Point Defects, Impurities, and their Diffusion in Silicon, Springer-Verlag, Vienna, 2004, https://doi.org/10.1007/978-3-7091-0597-9.

[30] H. Bracht, H.H. Silvestri, I.D. Sharp, E.E. Haller, Self- and foreign-atom diffusion in semiconductor isotope heterostructures. II. Experimental results for silicon, Phys. Rev. B 75 (2007) 35211, , https://doi.org/10.1103/PhysRevB.75.035211.

[31] E.L. Kennon, T. Orzali, Y. Xin, A. Vert, A.G. Lind, K.S. Jones, Deactivation of electrically supersaturated Te-doped InGaAs grown by MOCVD, J. Mater. Sci. 52 (2017) 10879–10885, https://doi.org/10.1007/s10853-017-1254-8.

[32] S.M. Hu, P. Fahey, R.W. Dutton, On models of phosphorus diffusion in silicon, J. Appl. Phys. 54 (1983) 6912–6922, https://doi.org/10.1063/1.331998.

[33] P.H. Keys, J.H. Li, E. Heitman, P.A. Packan, M.E. Law, K.S. Jones, Effect of extended defects on the enhanced diffusion of phosphorus implanted silicon, MRS Proc. 568 (1999) 199, , https://doi.org/10.1557/PROC-568-199.

[34] J. Li, P. Keys, J. Chen, M.E. Law, K.S. Jones, C. Jasper, Transient enhanced diffusion of phosphorus and defect evolution in P+ implanted Si, MRS Proc. 568 (1999) 175, , https://doi.org/10.1557/PROC-568-175.

[35] P.A. Packan, Physical Modeling of transient diffusion effects in silicon due to surface oxidation and ion-implantation, PhD Thesis, Department of Electrical Engineering, Stanford University, 1991.

[36] K.S. Jones, R.G. Elliman, M.M. Petravic, P. Kringhoj, Using doping superlattices to study transient-enhanced diffusion of boron in regrown silicon, Appl. Phys. Lett. 68 (1995) 3111, https://doi.org/10.1063/1.116439.

[37] D.J. Eaglesham, P.A. Stolk, H.J. Gossmann, J.M. Poate, Implantation and transient B diffusion in Si: the source of the interstitials, Appl. Phys. Lett. 65 (1994) 2305–2307, https://doi.org/10.1063/1.112725.

[38] J. Xu, V. Krishnamoorthy, K.S. Jones, M.E. Law, A comparison of boron and phosphorus diffusion and dislocation loop growth from silicon implants into silicon, J. Appl. Phys. 81 (1997) 107–111, https://doi.org/10.1063/1.363994.

[39] P.A. Stolk, D.J. Eaglesham, H.-J. Gossmann, J.M. Poate, Carbon incorporation in silicon for suppressing interstitial-enhanced boron diffusion, Appl. Phys. Lett. 66 (1995) 1370–1372, https://doi.org/10.1063/1.113204.

[40] P.A. Stolk, H.J. Gossmann, D.J. Eaglesham, D.C. Jacobson, J.M. Poate, H.S. Luftman, Trap-limited interstitial diffusion and enhanced boron clustering in silicon, Appl. Phys. Lett. 568 (1995) 568, https://doi.org/10.1063/1.114015.

[41] D.J. Eaglesham, T.E. Haynes, H.J. Gossmann, D.C. Jacobson, P.A. Stolk, J.M. Poate, Transient enhanced diffusion of Sb and B due to MeV silicon implants, Appl. Phys. Lett. 70 (1997) 3281–3283, https://doi.org/10.1063/1.119150.

[42] D. Mathiot, J. Pfister, High concentration diffusion of P in Si: a percolation problem? J. Phys. Lettres. 43 (1982) 453–459, https://doi.org/10.1051/jphyslet:019820043012045300.

[43] R.J. Bondi, S. Lee, G.S. Hwang, Theoretical characterization of silicon self-interstitial clusters in uniform strain fields, Phys. Rev. B - Condens. Matter Mater. Phys. 80 (2009) 1–10, https://doi.org/10.1103/PhysRevB.80.125202.

[44] R. Bondi, S. Lee, G. Hwang, Biaxial strain effects on the structure and stability of self-interstitial clusters in silicon, Phys. Rev. B 79 (2009) 104106, , https://doi.org/10.1103/PhysRevB.79.104106.

[45] H. Föll, M. Wilkens, A simple method for the analysis of dislocation loops by means of the inside-outside contrast on transmission electron micrographs, Phys. Status Solidi 31 (1975) 519–524, https://doi.org/10.1002/pssa.2210310223.